

Classification of Jaw Bone Cysts and Necrosis via the Processing of Orthopantomograms

Jan MIKULKA¹, Eva GESCHEIDTOVÁ¹, Miroslav KABRDA¹, Vojtěch PEŘINA²

¹ Dept. of Theoretical and Experimental Electrical Engineering, Brno University of Technology, Kolejní 2906/4, 612 00 Brno, Czech Republic

² Maxillary and Facial Surgery, The University Hospital Brno, Jihlavská 20, 625 00 Brno, Czech Republic

mikulka@feec.vutbr.cz, gescha@feec.vutbr.cz, xkabr00@stud.feec.vutbr.cz, vperina@seznam.cz

Abstract. The authors analyze the design of a method for automatized evaluation of parameters in orthopantomographic images capturing pathological tissues developed in human jaw bones. The main problem affecting the applied medical diagnostic procedures consists in low repeatability of the performed evaluation. This condition is caused by two aspects, namely subjective approach of the involved medical specialists and the related exclusion of image processing instruments from the evaluation scheme. The paper contains a description of the utilized database containing images of cystic jaw bones; this description is further complemented with appropriate schematic representation. Moreover, the authors present the results of fast automatized segmentation realized via the live-wire method and compare the obtained data with the results provided by other segmentation techniques. The shape parameters and the basic statistical quantities related to the distribution of intensities in the segmented areas are selected. The evaluation results are provided in the final section of the study; the authors correlate these values with the subjective assessment carried out by radiologists. Interestingly, the paper also comprises a discussion presenting the possibility of using selected parameters or their combinations to execute automatic classification of cysts and osteonecrosis. In this context, a comparison of various classifiers is performed, including the Decision Tree, Naive Bayes, Neural Network, k -NN, SVM, and LDA classification tools. Within this comparison, the highest degree of accuracy (85% on the average) can be attributed to the Decision Tree, Naive Bayes, and Neural Network classifiers.

Keywords

Image processing, image classification, follicular cyst, radicular cyst, live-wire, level set, OPG, RTG.

1. Introduction

A cyst is defined as a pathological cavity having its own capsule, epithelium, and liquid or semi-solid contents.

The wall of a cyst is formed by fibrous tissue; this wall behaves as a semi-permeable membrane, namely as a membrane unidirectionally permeable for the surrounding liquid. As a result of this behavior, the cyst gradually enlarges; in principle, expansive growth is a main characteristic of cysts [1].

Follicular cysts (Fig. 1) develop from the epithelium of a tooth bud and grow either between the exposed crown and the joined inner and outer epithelium of enamel or between both layers of the epithelium. The cysts may appear in consequence of primary defects in tooth bud development, and they may occur as individual or multiple objects [2]. In most cases, follicular cysts affect the mandibular region; large cysts often cause face-deforming bulges.

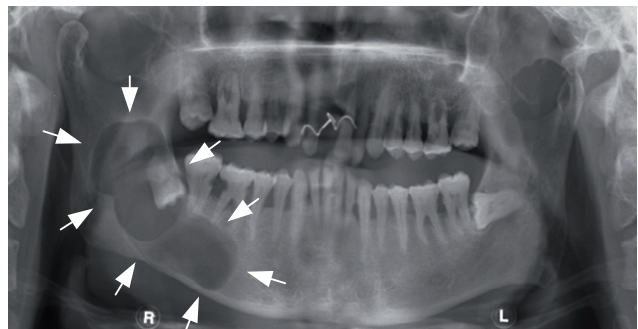


Fig. 1. An OPG image of a follicular cyst.

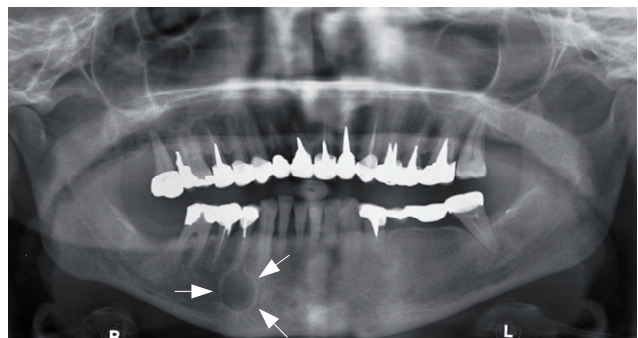


Fig. 2. An OPG image of a radicular cyst.

Radicular cysts (Fig. 2) are referred to as jaw bone cysts exhibiting the highest occurrence rates. It is assumed

that they appear due to inflammatory irritation of the epithelial cell rests of Malassez in the periodontal crevice; this irritation is caused by infected content of the radicular duct of a transverse tooth. The cysts are bound to pulpless teeth and may occur in patients of all age categories (most frequently between 30 and 40 years of age). In terms of elementary gender division of the patients, it is necessary to note that men tend to be affected rather more than women. The radicular cyst sac usually exhibits a round or oval shape [1].

The imaging of damaged jaws is very often realized by means of X-ray examination utilizing an orthopantomograph (OPG), which enables us to acquire panoramic images of entire jaw bones.

However, the imaging procedure can also be performed using other methods such as nuclear magnetic resonance (NMR). Even though this concrete technique is primarily intended for the imaging of soft tissues, its combination with current imaging sequences allows us to represent changes occurring in hard tissues, too. This application nevertheless exhibits a disadvantage consisting in image artifacts generated by changes in the susceptibility of the environment (factors such as implants or fillings), [3], [4]. Another applicable technique is electrical impedance tomography (EIT), which can be employed for the monitoring of tissue conductivity changes [5].

Generally, automatic classification of biomedical data constitutes a topical problem, and the main reason for the intensive development of automatic classification tools can be identified in the high degree of repeatability in disease diagnostics [6].

2. Image Database

A database containing 13 images of follicular cysts and 13 images of radicular cysts is currently available. In spite of its small size, the database is fully sufficient to enable the examination of these cysts. The following sections of this article present a description of training procedures applied to selected models; the training process allows us to classify the cysts into the two discussed categories. However, a necessary precondition for any refinement of the models consists in substantial enlargement of the database, which is a task depending on both the number of patients and the ability of the medical specialists to acquire image data.

3. Image Processing Chain

The actual image processing chain (Fig. 3) includes scanning via orthopantomograph, segmentation of the cystic area, and description of the area through local characteristics. These local characteristics of the segmented areas can be subsequently applied for setting the parameters of the model. The trained model will be used to facilitate automatized, computer-based classification of cysts.

3.1 Image Segmentation

Considering the aspects characteristic of the areas that represent jaw bone cysts and assuming the necessity to ensure correct demarcation of the given area before the actual acquisition of corresponding local descriptors, we cannot disregard the fact that the selection of a convenient segmentation method constitutes a vital step. In this context, it is necessary to note that OPG images are not very contrastive; simultaneously, cystic areas are characterized by blurred edges and inhomogeneous distribution of the pixel intensities. Thus, the use of traditional segmentation methods becomes rather problematic. Techniques based on global thresholding of the image are handicapped by adverse matching of the segmented area and the environment; moreover, these techniques may produce only partial segmentation. In view of the above-mentioned characteristics of OPG images, the analysis of area edges is also very prone to failures.

In order to attain the highest possible degree of automatization for the image classification system, we analyzed the results provided by several segmentation methods (thresholding, watershed, the Canny and Sobel edge detection, the region-based and edge-based level set methods). The aim of the analysis consisted in seeking a compromise

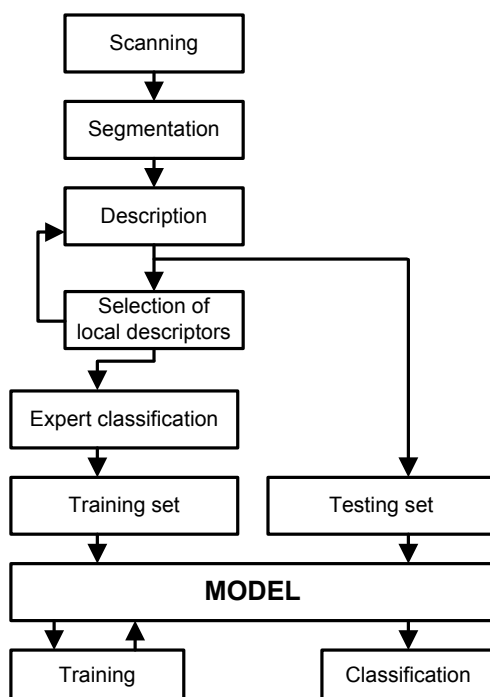


Fig. 3. The image processing chain designed to enable automatized classification of follicular and radicular cysts.

The presented article proposes a design of methods for the processing of OPG images and their implementation within automatized evaluation of follicular and radicular cysts. The aim of the design consists in the creation and training of a model based on real medical data; this model is intended for subsequent use in automatic classification of

between the rapidity of segmentation and the minimum necessary interaction of an expert.

Good results can be obtained via the method of active contours utilizing the level set (LS) approach [7], [8], [9]. The technique is based on the solution of the partial differential equation describing the curve which, in the initial phase of the segmentation process, is selected by the user as a simple piecewise linear curve located inside the area of interest. Through the subsequent solution of the equation toward the steady-state condition, there occurs a change of the curve shape or topology in order to facilitate the minimization of energy functional of the given segmentation problem. The most widely applied approaches to segmentation can be identified in the edge-based and the region-based methods. In the first of these techniques, the steady-state curve approximates the edges of the area of interest; in the second approach, the curve constitutes the boundary between two or more thresholds that divides the different mean values of the area intensities. For the purposes of our research, the edge-based segmentation approach is more convenient, mainly because the distribution of intensity within the cystic areas may be described as not very homogeneous. The edge-based level set segmentation method is formulated by the following partial differential equation:

$$\frac{d\phi}{dt} = g(|\nabla I|) \operatorname{div} \left(\frac{\nabla \phi}{|\nabla \phi|} \right) + \alpha g(|\nabla I|) |\nabla \phi| + \nabla g \cdot \nabla \phi \quad (1)$$

where I is the input image, α is the stabilizing constant ensuring convergence of the solution, and g is the function terminating the development of the level function at the location where the curve reaches the edge in the image. The function g is given by the relation:

$$g = \frac{1}{1 + |\nabla G_\sigma * I|^2} \quad (2)$$

The expression in the denominator of the function is the convolution of the input image with the Gaussian filter; therefore, a smoothed image is assumed. The result of segmentation in two selected cysts is shown in Figs. 4 and 5. While the left sections of both above-shown images indicate the initial curve, the right sections exhibit the shape of the curve in the steady state of the formula (1) solution.

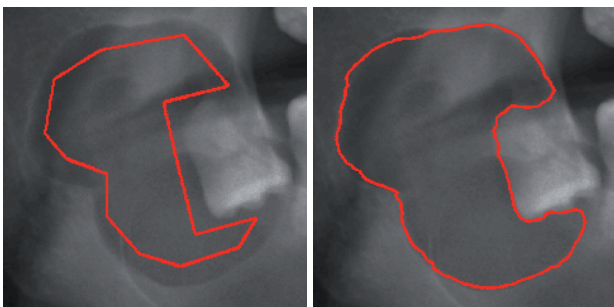


Fig. 4. Segmentation of a follicular cyst via the LS method.

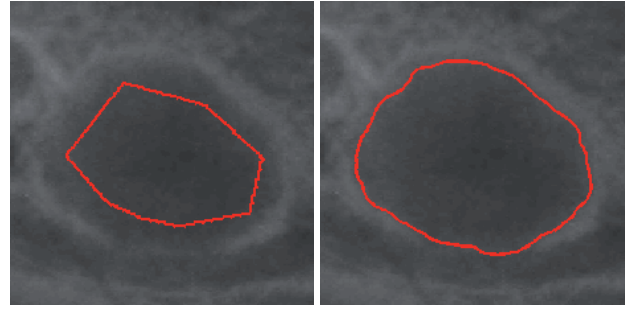


Fig. 5. Segmentation of a radicular cyst via the LS method.

Segmentation realized via the LS methods requires the user to execute the initialization via manually selecting the shape of the curve and locating it inside the cystic area. Even with the manual selection, the time period necessary for the execution of segmentation in the Matlab environment on a PC (Intel Core2 Quad 2,66 GHz, 4 GB RAM, Windows 7) did not exceed several tens of seconds. In order to stabilize the solution of the partial differential equation, the user is required to set convenient parameters for the segmentation; this fact may become rather problematic in practical applications of the system.

The remaining segmentation methods tested did not provide very good results, mainly owing to both the above-mentioned adverse characteristics of OPG images and the low contrast of the cystic area. In this context, the results obtained from segmentation via the watershed method [10] could be used as an example, Fig. 6. The aim of the processing was to carry out segmentation of the upper section of the follicular cyst from the OPG image shown in Fig. 1. The segment curve largely delimits the cyst exactly along its boundary; the result, however, would require further processing. In other cysts, which did not exhibit a contrast in the OPG images similar to the presented example, the watershed method utterly failed to satisfy the requirements.

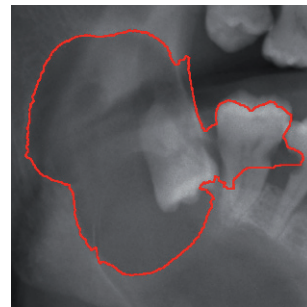


Fig. 6. Segmentation via the watershed method with the opening initialization realized via marking the segmented objects.

Based on a comparison of the segmentation quality and the time required for the processing, the semi-automatic live-wire segmentation method was selected as the most suitable option. The technique enables the user to carry out very fast manual demarcation of the area of interest via the shortest path algorithm. In the first phase of the process, convolution using the Sobel filter [11] is per

formed on the image; the filter allows us to sharpen the edges in the image. Then, the user marks the individual points, between which the optimum path is to be sought. This path will run along the edges of the region [12]. In the described case, the search for the shortest path is realized via the Dijkstra algorithm. The algorithm is finite (for any

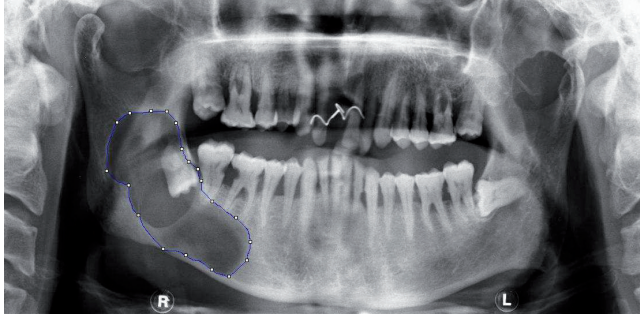


Fig. 7. Semi-automatic segmentation realized via the live-wire method – delimitation of a single area.

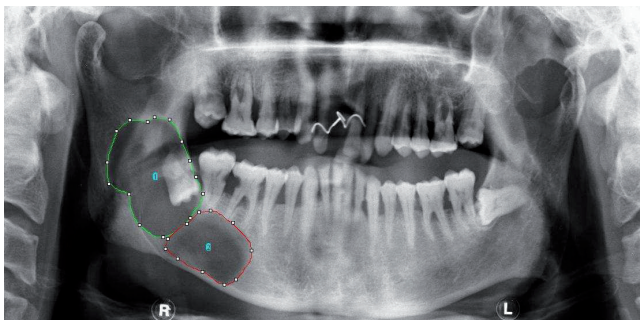


Fig. 8. Semi-automatic segmentation realized via the live-wire method – delimitation of a larger number of areas.

finite input, the algorithm will end), because in each cycle run the group of visited nodes is complemented with exactly one node. Thus, the number of cycle runs is limited by the number of vertices in the graph. Let us have graph G , in which we intend to find the shortest path. Then, let us determine that V is a set comprising all vertices of graph G and E is the set of all edges of graph G . The principle of the algorithm consists in that, for each vertex v from V , the algorithm retains the shortest length within all possible paths of access to the vertex. This value can be denoted as $d[v]$. At the initial stage, all the vertices exhibit the value of $d[v] = \infty$, excluding the initial vertex s , whose corresponding value is $d[s] = 0$. The infinity expresses an unknown path to the vertex. Further, the algorithm utilizes sets Z and N , where N contains the hitherto unvisited vertices and Z comprises their visited counterparts. The algorithm is cyclically repeated until the set N is empty. In each cycle of the algorithm, one vertex v_{min} is added from N to Z . This is the vertex exhibiting the lowest value $d[v]$ of all the vertices v from N . For each vertex u into which an edge leads from v_{min} (whose length is expressed as $l(v_{min}, u)$), the following algorithm is applied: if $(d[v_{min}] + l[v_{min}, u]) < d[u]$, then the value $d[v_{min}] + l[v_{min}, u]$ is assigned to $d[u]$. If this condition is not satisfied, there will not occur any consequence. When the algorithm ends, it will hold for each

vertex v from set V that the length of its shortest path from the initial vertex s is stored in $d[v]$ [12]. The live-wire method is suitable for the segmentation of images in which the area of interest, in each individual case, is located in a different position and assumes a different shape. For that reason, the described method appears to be the most convenient option for the image segmentation realized within our research. In the image, two or more areas can be marked simultaneously (Figs. 7 and 8).

3.2 Determination of Local Descriptors

The aim of further processing of the segmented images consists in acquiring local descriptors of the areas representing jaw bone cysts. In relation to the cystic areas, both the statistical evaluation of the distribution of pixel intensities and the determination of shape parameters were carried out via the ImageJ program. Within this phase of the research, we selected parameters to be evaluated in the presented set of images. These parameters were as follows: surface, mean value of the area intensity, standard deviation of the area pixel intensities, median of the area pixel intensities, modal value of the area pixel intensities, minimum and maximum values of the area pixel intensities, integral of the area pixel intensities, and shape characteristics of the segmented areas. In the last mentioned aspect, we selected the perimeter of the area, its circularity according to formula (3), the relation between the major and minor semi-axes of the fitted ellipse, the roundness according to relation (4), and the convexity according to relation (5):

$$C = 4 \cdot \pi \cdot \frac{S}{P^2}, \tag{3}$$

$$R = 4 \cdot \frac{S}{\pi \cdot a_{major}^2}, \tag{4}$$

$$X = \frac{S}{S_c} \tag{5}$$

where C is the circularity of the area, S is the surface of the area, P is the perimeter of the area, R is the roundness of the area, a_{major} is the length of the major semi-axis of the ellipse fitted into the area delimited by the original boundary points, X is the convexity of the area, and S_c is the surface of the convex area corresponding to the examined area.

The values presented in Tabs. 1 and 2 clearly indicate the difference between the follicular and the radicular cysts referred to in the introductory part of this study. While the follicular cysts exhibit a rather oblong shape, the radicular cysts are almost invariably of a circular character. Based on this parameter, it is possible to classify the cysts into two main groups:

- Circularity of the follicular cysts: 0.807 ± 0.149 ,
- Circularity of the radicular cysts: 0.932 ± 0.086 .

Parameter	Image/cyst												
	1	2	3	4	5	6	7	8	9	10	11	12	13
Area	47e3	75e3	28e3	66e3	30e2	25e3	83e3	19e3	60e3	16e3	14e4	36e3	11e4
Av. brightness	119.85	87.97	94.04	96.39	68.28	118.92	99.41	103.18	89.45	119.95	89.79	89.09	89.02
St. deviation	31.29	16.63	13.72	20.99	11.03	24.67	26.14	20.25	16.39	7.11	17.89	11.52	31.42
Bright. median	114	89	91	89	66	114	96	98	89	119	86	90	93
Modal value	112	90	87	74	61	109	100	87	99	118	86	91	51
Minimum	52	44	58	58	48	65	53	69	51	100	55	58	34
Maximum	222	170	171	155	135	204	219	172	143	151	193	135	212
Bright. integral	5648e3	6630e3	2642e3	6393e3	2096e3	3024e3	8259e3	1964e3	5441e3	1964e3	1325e4	3215e3	1052e4
Perimeter	802.04	1167.4	665.10	1246.1	611.74	632.82	1110.5	487.19	1028.9	459.21	1582.7	720.01	1594.1
Circularity	0.921	0.695	0.798	0.537	1.000	0.798	0.847	1.000	0.722	0.976	0.741	0.875	0.585
Semi-axes ratio	1.262	1.713	1.703	2.939	1.616	1.473	1.912	1.675	2.242	1.851	2.418	1.503	3.371
Roundness	0.793	0.584	0.587	0.340	0.619	0.679	0.523	0.597	0.446	0.540	0.414	0.665	0.297
Solidity	0.928	0.846	0.884	0.756	0.961	0.895	0.927	0.969	0.864	0.959	0.890	0.972	0.845

Tab. 1. Local descriptor values of the follicular cysts.

Parameter	Image/cyst												
	1	2	3	4	5	6	7	8	9	10	11	12	13
Area	13297	12910	70007	7761	73564	7697	18267	15910	3122	39535	27546	65250	38378
Av. brightness	81.71	105.12	98.16	94.62	89.78	82.45	93.61	67.87	57.34	81.02	97.13	114.97	85.67
St. deviation	15.00	13.52	18.00	13.81	15.29	5.18	12.11	13.62	4.56	22.51	15.80	18.31	13.73
Bright. median	79	105	93	94	85	82	93	66	57	83	97	114	83
Modal value	74	107	90	86	78	77	87	67	52	100	100	112	79
Minimum	53	71	68	68	52	69	67	40	48	42	60	62	60
Maximum	139	158	177	149	146	100	136	129	71	185	145	200	173
Bright. integral	1086e3	1357e3	6872e3	734e3	6604e3	634e3	1709e3	1079e3	179e3	3203e3	2675e3	7501e3	3287e3
Perimeter	396.78	398.54	978.29	314.76	1063.9	313.73	460.18	454.91	192.74	751.51	573.80	1024.7	780.38
Circularity	1	1	0.919	0.984	0.817	0.983	1	0.966	1	0.880	1	0.781	0.792
Semi-axes ratio	1.096	1.170	1.458	1.037	1.972	1.251	1.312	1.380	1.200	1.936	1.729	2.320	1.831
Roundness	0.913	0.855	0.696	0.964	0.507	0.799	0.762	0.724	0.833	0.516	0.578	0.431	0.546
Solidity	0.983	0.980	0.964	0.971	0.884	0.950	0.978	0.934	0.979	0.954	0.967	0.934	0.912

Tab. 2. Local descriptor values of the radicular cysts.

Quality improvement in the classification of the cysts may be achieved via selecting several parameters whose probability distribution does not overlap in any of the two types of cyst. As an example of these parameters, we could apply the ratio between the lengths of the major and the minor semi-axes of the fitted ellipse:

- Ratio between the lengths of semi-axes in the follicular cysts: 1.975 ± 0.613 ,
- Ratio between the lengths of semi-axes in the radicular cysts: 1.514 ± 0.401 .

Through subjective assessment of the values, it is also possible to select roundness as a suitable parameter enabling the classification of the cysts. Then, the related data are as follows:

- Roundness of the follicular cysts: 0.533 ± 0.159 ,
- Roundness of the radicular cysts: 0.767 ± 0.023 .

The family of parameters potentially applicable for the classification of cysts into the two discussed types also includes the cyst circumference (931.370 ± 387.689 in follicular cysts and 592.632 ± 295.213 in radicular cysts) and the integral of intensities in the area of the cyst ($5.465e6 \pm 3.548e6$ in follicular cysts and $2.840e6 \pm 2.558e6$ in radicular cysts). The parameters that could be influenced during the image acquisition (change of the image size, brightness degradation) are temporarily excluded from the classification process. The normalization of these parameters with respect to other invariant parameters will be incorporated in projected research.

It follows from the presented discussion of the values indicated in Tabs. 1 and 2 above that the automated system can be complemented with general classification of the cysts according to their types. The images evaluated by medical specialists will be correlated with the table values,

and a model facilitating the classification will be designed and trained.

3.3 Classification of Cysts

The classification of cysts involves several significant preconditions. In this context, let us emphasize mainly the selection of a proper model, which is an aspect influencing the quality of the classification process, and the choice of a convenient method for verifying the correctness of the training approach applied to the model. With respect to the latter prerequisite, we considered the generally small size of our image database and selected the cross-validation method as the most advantageous option. The tested results were acquired from the following models: Decision Tree, Naive Bayes, Neural Network, k-NN, SVM, and LDA.

We used the RapidMiner environment to perform the training and validation of the models; this software, although originally developed for the purposes of data mining [13], was gradually complemented with relevant tools to enable image mining [14].

The training of the model was realized in several steps. Initially, we loaded the data representing local descriptors of the segmented cysts. Then, the data were exploited to provide the values of parameters that will be further applied for the classification of the cysts; these parameters included the circularity, ratio of lengths of the axes, and roundness of the cysts. We utilized the discussed values as the training and testing data within the entire process of training the above-mentioned models. The splitting of the data into the training and testing groups was executed by the cross-validation system, which simultaneously evaluated the quality of the model.

Model	Follicular class accuracy	Radicular class accuracy
Decision Tree	81.8 %	88.9 %
Naive Bayes	88.9 %	81.8 %
Neural Network	81.8 %	88.9 %
SVM	75.0 %	87.5 %
LDA	87.5 %	75.0 %
k-NN	62.5 %	58.3 %

Tab. 3. Accuracy of the model evaluated via cross-validation.

The designed perceptron neural network consists of an input layer, two hidden layers, and an output layer. The input layer comprises 3 neurons, into which the measured parameter values are introduced. Then there are the two hidden layers (5 and 6 neurons) and the output layer, which comprises two neurons; at the output of these neurons, the logical values classifying the given cyst as radicular or follicular can be determined. The number of learning cycles in the back propagation algorithm was set to 500. The proposed SVM model utilizes the radial basis function with parameters $\gamma = 1$ and $C = 0$. For the k-NN algorithm,

we selected parameter $k = 3$, and Euclidean metrics was chosen to facilitate the measurement of distance.

In order to evaluate the accuracy of the model, we applied the above-mentioned 10-fold cross-validation approach with stratified sampling.

4. Other Classification Problems

The classification of cysts is the first problem to be solved within machine recognition of pathological tissues in OPG images. A similar yet significantly more complex problem consists in the recognition of jaw bone osteonecrosis and its classification according to the progression of damage to the tissue. Practically, necrotic tissues are classified into 4 types or stages:

- 1) Sclerotic region without the delimiting rim.
- 2) Tissue exhibiting signs of sequestration.
- 3) Lytic defect of the tissue.
- 4) Extensive cavity.

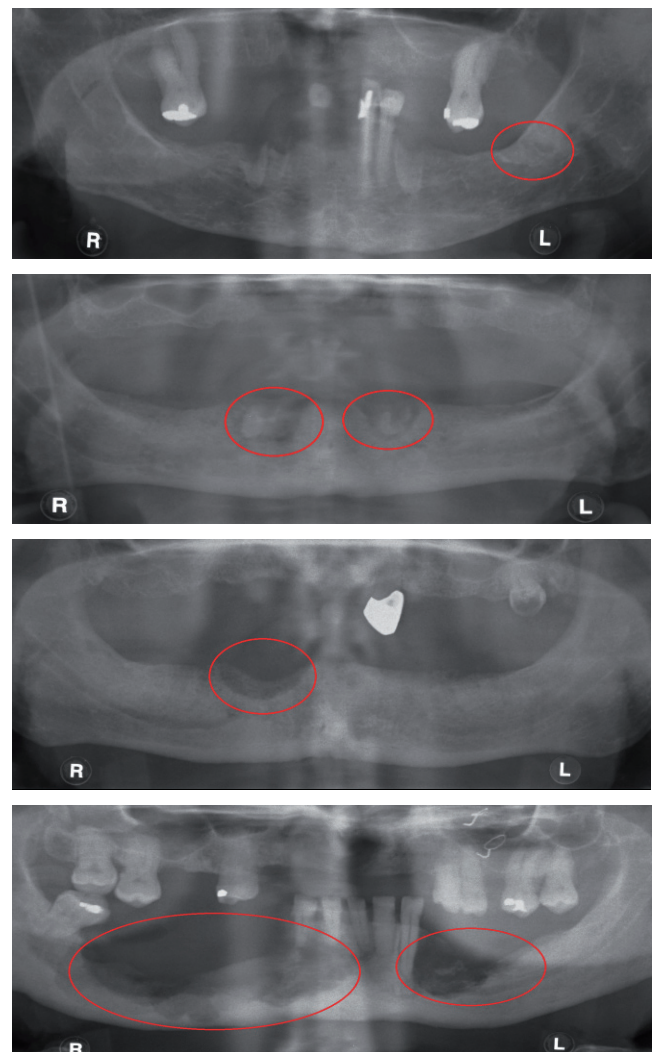


Fig. 9. Examples of osteonecrosis; individual stages of the disease are indicated down from top, 1-4.

Examples of osteonecrosis displayed by a panoramic dental X-ray apparatus are shown in Fig. 9.

The image processing chain is identical to that applied in the classification of cysts (Fig. 3). We used a set of images to evaluate selected parameters which could be utilized as a basis for the classification of the stage of necrosis. For the evaluation of this problem, the automatic approach is as significant as in the case of the classification of cysts. The reason for this significance clearly consists in the repeatability provided, because insufficient repeatability of the disease stage classification may cause problems such as distortion affecting the evaluation of efficiency related to the applied medication.

Segmentation of the image is performed manually. Within the process, the necrotic parts are manually demarcated to enable the determination of local descriptors. The evaluation results for these descriptors are summarized in Tab. 4.

	1	2	3	4
Area	34.8 ±10.8	47.3 ±16.3	57.5 ±15.7	158.2 ±195.0
Av. brightness	111.3 ±11.2	109.1 ±22.2	91.0 ±6.3	87.5 ±11.9
St. deviation	10.1 ±4.2	13.2 ±5.8	8.1 ±1.0	12.8 ±5.8
Modal value	114.5 ±9.7	101.2 ±30.1	89.5 ±5.0	81.8 ±19.4
Minimum	81.3 ±15.0	74.8 ±25.0	69.5 ±0.7	58.0 ±11.3
Maximum	139.0 ±18.5	171.2 ±41.3	121.0 ±5.7	135.8 ±25.8
Bright. median	111.75 ±10.6	108.4 ±23.0	90.0 ±5.7	87.8 ±13.3

Tab. 4. Local descriptor values for the necrotic tissues.

The classification of the stage of osteonecrosis progression in jaw bone tissues is proposed in a follow-up study. At this point, we could also refer to automatic recognition of necrotic areas, which constitutes a minor yet very interesting problem. An apparatus enabling such type of recognition would considerably improve the quality of diagnostics provided by hospital departments of radiology, where primary description of the represented tissues is realized.

As indicated in Tab. 4, the group of factors to be utilized in the classification of the disease stage comprises the size of the necrotic tissue surface (increasing with the progression of the tissue damage) and the average intensity of the necrotic area (decreasing with the progression of the tissue damage). Further, correlation can be identified between the stage of damage to the tissue and modal value of the intensity, minimum value of the intensity, and median of the intensity. Tab. 5 contains a summary of Pearson's correlation coefficients applied to the stage of the disease and the estimates of mean values of selected image parameters in the necrotic areas.

The set of selected parameters includes the following elements:

- $\rho_{X, AREA}$ – correlation between the stage of osteonecrosis and the mean value estimate for the surface of the necrotic areas,
- $\rho_{X, MEAN}$ – correlation between the stage of osteonecrosis and the mean value estimate for the brightness of the necrotic areas,
- $\rho_{X, MODAL}$ – correlation between the stage of osteonecrosis and the modal value of brightness of the necrotic areas,
- $\rho_{X, MIN}$ – correlation between the stage of osteonecrosis and the minimum value of brightness of the necrotic areas,
- $\rho_{X, MEDIAN}$ – correlation between the stage of osteonecrosis and the median of brightness of the necrotic areas.

$\rho_{X, AREA}$	$\rho_{X, MEAN}$	$\rho_{X, MODAL}$	$\rho_{X, MIN}$	$\rho_{X, MEDIAN}$
0.8684	-0.9461	-0.9933	-0.9845	-0.9446

Tab. 5. Correlation coefficients between the stage of osteonecrosis and selected image parameters.

In Tab. 5, direct relation between selected parameters and the stage of osteonecrosis is presented. The parameters will be applied in the process of training the model for machine classification of necrosis.

5. Conclusions

The article contains a description of basic research in the processing of OPG images acquired to facilitate the classification of jaw bone cysts and necrosis.

Jaw bone cysts can be classified into two groups: follicular and radicular. The image processing results indicated in Tabs. 1 and 2 show that binary classification of cysts can be performed using a combination of several parameters (circularity, radius of semi-axes of the fitted ellipse, surface of the cystic area). An algorithm (Fig. 3) enabling the classification of the disease stage was designed. Six different tools (Decision Tree, Naive Bayes, Neural Network, SVM, LDA, k-NN) were chosen to perform the categorization of jaw bone cysts into the given classes. Based on evaluation of the accuracy rates achieved by the above-listed classifiers, we identified the simple Decision Tree method, the Naive Bayes model, and the neural network approach as the most appropriate classification tools. The concrete accuracy rates obtained via these classifiers were 81.8 % for the follicular and 88.9 % for the radicular cyst classes. However, it is necessary to note that, considering the comparatively small number of available images, these values are not prescriptive as regards the selection of a generally suitable model. Yet the training and validation of the models together with the discussion of the results shown in Tabs. 1 and 2 fully allow us to claim that cysts can be effectively classified via the machine binary approach.

Within the second part of the paper, the problem of classifying jaw bone necrosis is described. For this form of pathological tissue, we selected and examined certain local descriptor values, namely surface, average intensity, standard deviation of the intensities, modal value of the intensities, minimum and maximum values of the intensities, and median of the intensities. These values (shown in Tab. 4) were determined for each of the four necrotic tissue stages. The increase or decrease of the individual values in relation to the necrosis stage enables us to predict the possibility of successful classification of the disease. In order to exemplify this fact, we could refer to the modal value of intensity inside a necrotic area. In the necrotic tissue concerned, the modal values of intensity are 114.5 ± 9.7 at the initial stage and 81.8 ± 19.4 in a large nidus (at the final stage). Generally, owing to mutual overlapping between the distribution of modal values and other local descriptors, it is not possible to classify the stage of necrosis using only a single parameter; moreover, the inclusion of more descriptors into the classification process will increase the classification accuracy. As is obvious from the values shown in Tab. 5, significant correlation can be found between the stage of osteonecrosis and selected parameters, namely mean value of the intensities ($\rho_{X, \text{Mean}} = -0.941$), modal value of the intensities ($\rho_{X, \text{Modal}} = -0.9933$), minimum value ($\rho_{X, \text{Min}} = -0.9845$), and median of the intensities ($\rho_{X, \text{Median}} = -0.9446$). Also, the absolute value of Pearson's correlation coefficient approaching 1 denotes a high degree of correlation between the values, while the coefficient value of 0 signifies zero relation.

Acknowledgements

This work was partially supported by the project CZ.1.07/2.3.00/30.0039 of Brno University of Technology and Grant no. GAP102/11/0318.

References

- [1] PAZDERA, J. *The Basis of Oral Surgery*. UP Olomouc, 2011. ISBN 978-80-244-2660-0.
- [2] ČERNOCHOVÁ, P. *The Diagnosis of Impacted Teeth*. Prague: Grada Publishing, 2006, ISBN 80-247-1269-5.
- [3] MARCOŇ, P., BARTUŠEK, K., POKLUDOVÁ, M., DOKOUPIL, Z. Magnetic susceptibility measurement using 2D magnetic resonance imaging. *Measurement Science and Technology*, 2011, vol. 2011, no. 22, p. 1-8. ISSN: 0957- 0233.
- [4] MARCOŇ, P., BARTUŠEK, K., GESCHEIDTOVÁ, E., DOKOUPIL, Z. Diffusion MRI: magnetic field inhomogeneities mitigation. *Measurement Science Review*, 2012, vol. 12, no. 5, p. 205-212. ISSN: 1335- 8871.
- [5] DĚDKOVÁ, J., OSTANINA, K. Two- dimensional tissue image reconstruction based on magnetic field data. *Radioengineering*, 2012, vol. 21, no. 3, p. 917-922. ISSN: 1210- 2512.

- [6] AYDEMIR, O., KAYIKCIOGLU, T. Wavelet transform based classification of invasive brain computer interface data. *Radioengineering*, 2011, vol. 20, no. 1, p. 31-38. ISSN: 1210-2512.
- [7] LI, CH., XU, CH., GUI, CH., FOX, M. D. Level set evolution without re-initialization: A new variational formulation. In *IEEE Computer Society Conference on Computer Vision and Pattern Recognition (CVPR 2005)*. San Diego (CA, USA), 20-26 June 2005.
- [8] MIKULKA, J., GESCHEIDTOVÁ, E., BARTUŠEK, K. Soft-tissues image processing: comparison of traditional segmentation methods with 2D active contour methods. *Measurement Science Review*, 2012, vol. 12, no. 4, p. 153-161. ISSN: 1335- 8871.
- [9] MIKULKA, J., GESCHEIDTOVÁ, E., BARTUŠEK, K. Processing of MR slices of human liver for volumetry. In *PIERS 2010 in Xi'an Proceedings*. 2010, p. 202-204. ISBN: 978-1-934142-12- 7.
- [10] CUTRONA, J., BONNET, N. Two methods for semi-automatic image segmentation based on fuzzy connectedness and watersheds. In *Proceedings of the IASTED International Conference on Visualization, Imaging and Image Processing (VIIP 2001)*. Marbella (Spain), September 2001.
- [11] HLAVÁČ, V., ŠONKA, M. *Computer Vision*. Prague: Grada Publishing, 1992. ISBN 80-85424-67-3 (in Czech).
- [12] BAGGIO, D. L. *GPGPU Based Image Segmentation Livewire Algorithm Implementation*. [Online] Technological Institute of Aeronautics, Sao José dos Campos, 2007. Available at: <http://gpuwire.googlecode.com/files/Master%20Thesis%20-%20Updated%20February%2015th.pdf>
- [13] BURGET, R., UHER, V., MASEK, J. Trainable segmentation based on local-level and segment-level feature extraction. In *Proceedings of the Ninth IEEE International Symposium on Biomedical Imaging: From Nano to Macro (ISBI'12)*. Barcelona (Spain), May 2-5, 2012.
- [14] UHER, V., BURGET, R. Automatic 3D segmentation of human brain images using data-mining techniques. In *35th International Conference on Telecommunications and Signal Processing TSP2012*. Prague (Czech Rep.), July 2012.

About Authors ...

Jan MIKULKA received the PhD degree in Electrical Engineering from Brno University of Technology, Faculty of Electrical Engineering and Communication in 2011. His research work is centered on a wide variety of problems within NMR imaging, such as image segmentation and classification.

Eva GESCHEIDTOVÁ received the Ing. (MSc) degree in Electrical Engineering in 1974 and the CSc (PhD) degree in 1983, both from Brno University of Technology. In 1974, she joined the Dept. of Theoretical and Experimental Electrical Engineering, Faculty of Electrical Engineering and Informatics, Brno University of Technology. Ms. Gescheidtová is a full-time lecturer in electrical measurement. Her research work is concentrated on problems of electrical measurement, nuclear magnetic resonance, and signal processing.

Miroslav KABRDA received the MSc degree in Electrical Engineering from Brno University of Technology in 2012. His work and thesis were focused on problems of OPG imaging and image processing, mainly features extraction and image classification.

Vojtěch PEŘINA received the MD and the PhD degrees in stomatology from Masaryk University, Faculty of Medicine, in 2002 and 2010. His work and thesis were focused on the analysis of problems within bone mineral density evaluation and osteoporosis.